Lithium-Ion Battery State Estimation for a Single Particle Model with Intercalation-Induced Stress

Dong Zhang, Satadru Dey, Scott J. Moura

***Abstract*— This paper develops a nonlinear observer for lithium-ion battery electrode particle stress and state-of-charge (SOC) estimation using the single particle model (SPM) coupled with mechanical stress. Particle fracture due to stress generation is a critical mechanism causing capacity fade, and thus reducing battery life. The stress sub-model captures stress developed during lithium ion intercalation and deintercalation. State estimation based on coupled SPM and mechanical stress model is particularly challenging because the coupled model is given by nonlinear partial differential equations (PDEs). We address this problem by reducing the coupled model to a system of nonlinear ordinary differential equations (ODEs), and then apply nonlinear observer design methods. The key novelty of this design is a nonlinear internal state estimation algorithm, from which the internal stress can be monitored from current and terminal voltage measurements only. Simulation studies illustrate the performance of the proposed estimation scheme.**

NOMENCLATURE

α^j	Charge transfer coefficient [-]
ν^j	Poisson's ratio [-]
Ω^j	Partial molar volume [mol/m^3]
σ_h^j	Hydrostatic stress [MPa]
$\tilde{c}_s^j$	Concentration change from initial value [mol/m^3]
ε_s^j	Volume fraction of solid phase [-]
A	Cell cross sectional area [m^2]
a^j	Specific interfacial surface area [m^2/m^3]
c_e^0	Li-ion concentration in electrolyte phase [mol/m^3]
$c_{s,\max}^j$	Max Li-ion concentration in solid phase [mol/m^3]
c_{ss}^j	Li-ion concentration at particle surface [mol/m^3]
c_s^j	Solid phase lithium-ion concentration [mol/m^3]
D_s^j	Solid phase diffusion coefficient [m^2/sec]
E^j	Young's Modulus [GPa]
F	Faraday's constant [C/mol]
I	Applied current [A]
i_n^j	Particle surface current density [A/m^2]
j	Negative (-) or positive (+) electrodes [-]
k^j	Charge transfer reaction rate [A$\cdot$m$^{2.5}$/mol$^{1.5}$]
L^j	Electrode thickness [m]
R	Universal gas constant [J/mol-K]
r	Radial coordinate [m]
R_f	Contact film resistance [Ω]
R_s^j	Particle radius [m]
T	Battery cell temperature [K]
U^j	Open circuit potential [V]

Dong Zhang, Scott J. Moura are with Energy, Controls, and Applications Lab (eCAL) in Civil and Environmental Engineering, University of California Berkeley, CA 94720, USA (e-mail: {dongzhr, smoura}@berkeley.edu)

Satadru Dey is with Department of Electrical Engineering, University of Colorado Denver, CO 80204, USA (email: satadru.dey@ucdenver.edu)

I. INTRODUCTION

Lithium-ion (Li-ion) batteries have drawn significant research attention, owing to their various benefits for energy storage applications. Nonetheless, degradation and safe operation of Li-ion batteries become critical as the usage of Li-ion batteries gets ubiquitous. To address this problem, a battery management system (BMS) implements real-time control and estimation algorithms to enhance performance while improving safety [1]. One of the important functions of a BMS is battery state-of-charge (SOC) and state-of-health (SOH) estimation. However, SOC and SOH estimation is intricate due to (i). limited measurements, (ii). complex electrochemical-thermal-mechanical physics, and (iii). limitations of control theory - especially for nonlinear partial differential equation models.

Battery models are typically used in a BMS for estimating internal states based on measured current, voltage and temperature [2], [3]. High-fidelity electrochemical models, e.g. [2], capture the underlying physical and chemical processes, yet their mathematical structures are often complicated for control/estimation design. This motivates model reduction of full order electrochemical models. Among the numerous reduced order models, the single particle model (SPM) is the most commonly used. The SPM is derived from the full order electrochemical model, and hence it inherits some important properties. Each electrode of the SPM is assumed to be a single spherical particle and the current distribution is uniform across both electrodes. Moreover, the electrolyte concentration is assumed constant in space and time [3]. Various SOC/SOH estimation technique has been developed based on the SPM. A Kalman filter was designed for SOC estimation in [4], [5]. Moura *et al.* created an adaptive PDE observer for combined SOC and SOH estimation in [6]. An important drawback of the SPM is that it does not accurately predict voltage at high C-rate, since the electrolyte dynamics are neglected. In order to compensate this, models that combine the SPM with other components are proposed, e.g. electrolyte dynamics [7]–[9].

In recent years, battery SOH has gained increased focus due to concerns over battery safety and life. Numerous factors contribute toward battery aging, e.g. capacity fade and resistance growth. See [10] for a particularly excellent review. A crucial capacity fade mechanisms is particle fracture due to intercalation and deintercalation-induced stress [11]. The stress field generated inside the particles affects the energy of the subsequent intercalated lithium ions, leading to a modified diffusion phenomenon from the stress-free

scenario [12]. A particle can fracture if the generated stress exceeds the yielding stress of the material [13], which depends on both radial and tangential stresses [14], [15]. This phenomenon motivates the development of models to describe stress influences. Seminal work conducted by Christensen and Newman created mathematical models to capture volume expansion and contraction during lithium insertion [16]. Later, models that combine the SPM with diffusion-induced stress was introduced in [17], relying on an analogy to thermal stress. An interesting BMS application of these models is introduced in [13], where the authors performed optimal charging under stress constraints.

In summary, there now exists a keen interest to address the state-of-health estimation problem, and recent model developments on diffusion induced-stress can be enabling. However, no work currently exists on state estimation with coupled SPM-stress models. In the present work, we design a nonlinear observer based on this model to estimate the electrode particle stress profile and bulk SOC from current and voltage measurements. The internal stress developed inside the electrode particle can be monitored in real time to ensure safe operation.

The remainder of the paper is organized as follows: Section II presents the battery single particle model with intercalation-induced stress. Section III discusses model reduction, state-space formulation, and nonlinear observer design with stability analysis. The estimator is demonstrated via simulation studies in Section IV. Conclusions are drawn in Section V.

II. Model Description

Figure 1 portrays the concept of the SPM. In the full order electrochemical model [18], lithium ion transports in the solid and electrolyte phase. The key idea of the SPM is that the solid phase of each electrode can be modeled as a single spherical particle, and lithium ion concentration in electrolyte phase is assumed to be constant in space and time [6]. The SPM specifically does not include mechanical responses, whose effect on diffusion becomes significant when the material has high modulus and high partial molar volume. The model equations for the coupled SPM and mechanical stress presented here closely follow the paper by Zhang *et al.* [17].

For the case of a spherical particle, the intercalation of lithium ions in the solid phase is modeled as a process due to diffusion and stress generation, given by

$$\frac{\partial c_s^j}{\partial t} = D_s^j\left[\frac{\partial^2 c_s^j}{\partial r^2} - \frac{\Omega^j}{RT}\frac{\partial c_s^j}{\partial r}\frac{\partial \sigma_h^j}{\partial r} - \frac{\Omega^j c_s^j}{RT}\left(\frac{\partial^2 \sigma_h^j}{\partial r^2} + \frac{2}{r}\frac{\partial \sigma_h^j}{\partial r}\right)\right], \tag{1}$$

with the boundary condition

$$-D_s^j\left(\frac{\partial c_s^j}{\partial r} - \frac{\Omega^j c_s^j}{RT}\frac{\partial \sigma_h^j}{\partial r}\right) = \frac{i_n^j}{F}, \tag{2}$$

where $c_s^j(r,t) : [0, R_s^j] \times \mathbb{R}^+ \to \mathbb{R}$ maps the radial position and time to solid phase lithium concentration in electrode j, and $\sigma_h^j(r,t) : [0, R_s^j] \times \mathbb{R}^+ \to \mathbb{R}$ maps the radial position and time to hydrostatic stress in electrode j. The stress tensor consists of radial stress σ_r and tangential stress σ_t:

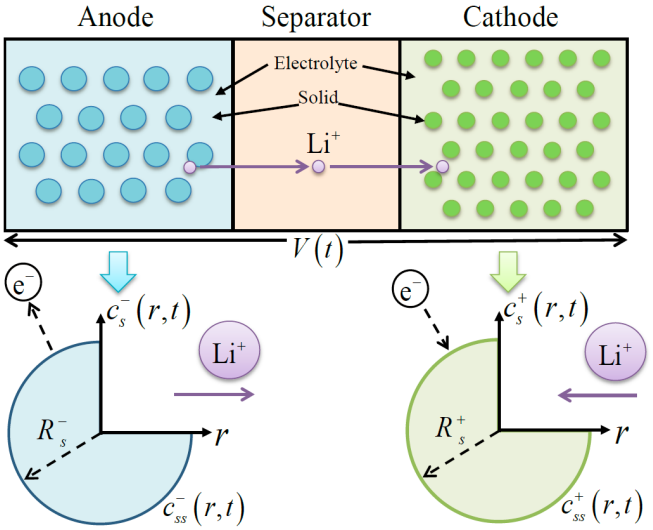

Fig. 1: Sketch of the Single Particle Model concept

$$\sigma_r^j = \frac{2\Omega^j E^j}{3(1-\nu^j)}\left[\frac{1}{(R_s^j)^3}\int_0^{R_s^j} \tilde{c}_s^j r^2 dr - \frac{1}{r^3}\int_0^r \tilde{c}_s^j \rho^2 d\rho\right], \tag{3}$$

$$\sigma_t^j = \frac{\Omega^j E^j}{3(1-\nu^j)}\left[\frac{2}{(R_s^j)^3}\int_0^{R_s^j} \tilde{c}_s^j r^2 dr + \frac{1}{r^3}\int_0^r \tilde{c}_s^j \rho^2 d\rho - \tilde{c}_s^j\right]. \tag{4}$$

The hydrostatic stress is a weighted sum of σ_r and σ_t:

$$\sigma_h^j = \frac{\sigma_r^j + 2\sigma_t^j}{3} = \frac{2\Omega^j E^j}{9(1-\nu^j)}\left[\frac{3}{(R_s^j)^3}\int_0^{R_s^j} \tilde{c}_s^j r^2 dr - \tilde{c}_s^j\right]. \tag{5}$$

Substituting (5) into (1) yields

$$\frac{\partial c_s^j}{\partial t} = D_s^j\left[(1+\theta^j c_s^j)\left(\frac{\partial^2 c_s^j}{\partial r^2} + \frac{2}{r}\frac{\partial c_s^j}{\partial r}\right) + \theta^j\left(\frac{\partial c_s^j}{\partial r}\right)^2\right], \tag{6}$$

where $\theta^j = (\Omega^j/RT)[(2\Omega^j E^j)/9(1-\nu^j)]$ is a constant depending on electrode material mechanical properties. The boundary condition is obtained by substituting (5) into (2):

$$-D_s^j\left(1+\theta^j c_s^j(R_s^j,t)\right)\frac{\partial c_s^j}{\partial r}(R_s^j,t) = \frac{i_n^j}{F}, \tag{7}$$

where the current density i_n^j is proportional to the input current by the relation $i_n^j = \pm I/a^j A L^j$. For well-posedness, the Neumann boundary condition at $r = 0$ is required:

$$\frac{\partial c_s^j}{\partial r}(0,t) = 0. \tag{8}$$

Therefore, the governing equations for the solid phase lithium ion concentration with intercalation-induced stress is described by (6)-(8).

The output terminal voltage is a function of solid phase surface concentration, electric overpotential, and Butler-

Volmer kinetics:

$$\begin{aligned} V_T(t) =& \frac{RT}{\alpha^+ F}\sinh\left(\frac{-I(t)}{2a^+AL^+i_0^+(c_{ss}^+(t))}\right) \\ &- \frac{RT}{\alpha^- F}\sinh\left(\frac{I(t)}{2a^-AL^-i_0^-(c_{ss}^-(t))}\right) \\ &+ U^+(c_{ss}^+(t)) - U^-(c_{ss}^-(t)) + R_f I(t), \end{aligned} \tag{9}$$

where the exchange current density i_0^j is

$$i_0^j(c_{ss}^j) = k^j\sqrt{c_e^0 c_{ss}^j(t)(c_{s,\max}^j - c_{ss}^j(t))}, \tag{10}$$

$$c_{ss}^j(t) = c_s^j(R_j, t). \tag{11}$$

$U^+(\cdot)$ and $U^-(\cdot)$ in Eq. (9) are the equilibrium potentials of positive and negative electrode material as functions of solid phase surface concentrations.

An important property of the coupled SPM-stress model is given by the following proposition, which will be leveraged for model reduction in the next section.

Proposition 1 (Conservation of solid-phase lithium)**.** *The moles of lithium in the solid phase is conserved. Mathematically,* $\frac{d}{dt}(n_{Li}(t)) = 0$ *where*

$$n_{Li}(t) = \sum_{j\in\{+,-\}} \frac{\varepsilon_s^j L^j A}{\frac{4}{3}\pi(R_s^j)^3}\int_0^{R_s^j} 4\pi r^2 c_s^j(r,t)dr. \tag{12}$$

Proof: The proof is straight-forward. Differentiate (12) with respect to t, substitute (6), apply integration by parts and the boundary conditions (7) and (8).

III. State Observer Design

This section presents observability analysis, model reduction, and the nonlinear observer design procedures. The convergence of the proposed estimation scheme is mathematically analyzed by Lyapunov stability theory.

A. Observability and Model Reduction

The observability of (6) (both anode and cathode dynamics) from voltage measurements (9) in the linear sense can be checked by the following procedure [19]:

1) Approximate PDEs with ODEs using finite difference method
2) Linearize the nonlinear ODEs about the states at the equilibrium to produce matrix A_l
3) Linearize the nonlinear output function about the states at the equilibrium to produce matrix C_l
4) Compute the observability matrix for the pair (A_l, C_l), and check the rank

The above calculation reveals that the PDEs given by (6) with boundary conditions (7)-(8) is not observable from the voltage measurements. Hence, we adopt the model reduction technique from [6], where the cathode diffusion dynamics are approximated by its equilibrium. This reduction produces a reduced system where the states are locally observable in the linear sense. The equilibrium of the cathode states can be calculated using the property in (12):

$$c_{ss}^+ = \frac{1}{\varepsilon_s^+ L^+ A}\Big(n_{Li} - \varepsilon_s^- L^- A c_{ss}^-\Big), \tag{13}$$

and the output function (9) can be adjusted accordingly:

$$\begin{aligned} V_T(t) =& \frac{RT}{\alpha^+ F}\sinh\left(\frac{-I(t)}{2a^+AL^+i_0^+(\gamma c_{ss}^-(t)+\delta)}\right) \\ &- \frac{RT}{\alpha^- F}\sinh\left(\frac{I(t)}{2a^-AL^-i_0^-(c_{ss}^-(t))}\right) \\ &+ U^+(\gamma c_{ss}^-(t)+\delta) - U^-(c_{ss}^-(t)) + R_f I(t), \end{aligned} \tag{14}$$

where $\gamma = -(\varepsilon_s^- L^-)/(\varepsilon_s^+ L^+)$ and $\delta = n_{Li}/(\varepsilon_s^+ L^+ A)$. The reduced system is then modeled by diffusion equation (6) with boundary conditions (7)-(8) for the anode (c_s^--system), and output function (14). Local observability in the linear sense for the reduced system can be verified by the procedure introduced previously.

B. State-Space Model Formulation and Analysis

The central difference method is used for discretizing the PDEs into ODEs. Henceforth, we will only consider dynamical equations and boundary conditions for anode, and let $c = c_s^-$, $D = D_s^-$, $R_s = R_s^-$, $a = a^-$, $L = L^-$, and $\theta = \theta^-$ to simplify notation. Suppose N nodes are used for discretization in the r direction, and $\Delta r = R_s/N$. Define the time constant

$$\tau = \frac{D}{(\Delta r)^2}. \tag{15}$$

The system of ODE for the internal nodes of the anode diffusion dynamics are

$$\begin{aligned} \frac{\partial c_i}{\partial t} =& \tau\Bigg[(1+\theta c_i)(c_{i-1} - 2c_i + c_{i+1}) \\ &+ \left(\frac{2}{i} + \theta\frac{c_{i+1}-c_{i-1}}{2} + \frac{2\theta}{i}c_i\right)\left(\frac{c_{i+1}-c_{i-1}}{2}\right)\Bigg], \end{aligned} \tag{16}$$

where $i \in \{1, 2, \cdots, N-1\}$. At the right boundary point $i = N$, the method of imaginary points is utilized to discretize the governing equations:

$$\begin{aligned} \frac{\partial c_N}{\partial t} =& \tau\left[(1+\theta c_N)\left(c_{N-1} - c_N - \frac{I\cdot\Delta r}{DFaAL(1+\theta c_N)}\right)\right] \\ &+ \tau\left[\frac{1}{N} + \frac{\theta}{4}\left(c_N - c_{N-1} - \frac{I\cdot\Delta r}{DFaAL(1+\theta c_N)}\right)\right. \\ &\left. + \frac{\theta}{N}c_N\right]\cdot\left(c_N - c_{N-1} - \frac{I\cdot\Delta r}{DFaAL(1+\theta c_N)}\right). \end{aligned} \tag{17}$$

Remark 1. Equation (33) in [17] provides a particular PDE for solving lithium concentration at the center of the sphere considering the singularity at $r = 0$. However, including this equation in the state-space model leads to unobservable condition. We tackle this problem by simply ignore this equation and set $c_0 = c_1$ based on forward difference method at $r = 0$, where the dynamics of c_1 is expressed by (16). In this way, the observability in the linear sense is guaranteed.

The state-space model can be written in the following form based on (16) and (17):

$$\begin{aligned} \dot{x} &= \mathcal{A}x + f(x,u), \\ y &= h(c_N, u), \end{aligned} \tag{18}$$

where the states $x = \begin{bmatrix} c_1 & c_2 & ... & c_N \end{bmatrix}^T \in \mathbb{R}^N$, input $u = I \in \mathbb{R}$ is the applied current, output terminal voltage $y = h(x_N, u) = V_T \in \mathbb{R}$, nonlinear function $f(x,u) = \begin{bmatrix} f_1(x) & f_2(x) & ... & f_{N-1}(x) & f_N(x,u) \end{bmatrix}^T \in \mathbb{R}^N$, and matrix $\mathcal{A} \in \mathbb{R}^{N\times N}$. Following the derivation from (16), we have

$$\mathcal{A} = \begin{bmatrix} -2 & 2 & 0 & \cdots & \cdots & 0 \\ \frac{1}{2} & -2 & \frac{3}{2} & \cdots & \cdots & 0 \\ 0 & \frac{2}{3} & -2 & \cdots & \cdots & 0 \\ \vdots & \vdots & \vdots & \ddots & \ddots & \vdots \\ 0 & 0 & 0 & \cdots & -2 & \frac{N}{N-1} \\ 0 & 0 & 0 & \cdots & \frac{N-1}{N} & -\frac{N-1}{N} \end{bmatrix}, \quad (19)$$

and

$$f(x,u) = \tau \cdot \theta \cdot \begin{bmatrix} 2c_1(c_2-c_1) + \frac{(c_2-c_1)^2}{4} \\ c_2(c_1-2c_2+c_3) + \frac{(c_3-c_1)^2}{4} + \frac{c_2(c_3-c_1)}{2} \\ \vdots \\ c_i(c_{i-1}-2c_i+c_{i+1}) + \frac{(c_{i+1}-c_{i-1})^2}{4} + \frac{c_i(c_{i+1}-c_{i-1})}{2} \\ \vdots \\ f_N(c_{N-1}, c_N, u) \end{bmatrix} \quad (20)$$

where

$$\begin{aligned} f_N = & -\frac{N+1}{\theta N}\frac{I\cdot\Delta r}{DFaAL(1+\theta c_N)} \\ & + c_N\left[c_{N-1} - c_N - \frac{I\cdot\Delta r}{DFaAL(1+\theta c_N)}\right] \\ & + \left[\frac{1}{4}\left(c_N - c_{N-1} - \frac{I\cdot\Delta r}{DFaAL(1+\theta c_N)}\right) + \frac{1}{N}c_N\right]\times \\ & \left[c_N - c_{N-1} - \frac{I\cdot\Delta r}{DFaAL(1+\theta c_N)}\right]. \end{aligned} \quad (21)$$

The state estimation problem is to design an observer system to reconstruct the unknown states x in (18) with the knowledge of output measurement y and input u.

Assumption 1. It has been verified by numerous literature, e.g. [20], that the nonlinear output function $h(c_N, u)$ is strictly increasing with respect to the state c_N. Therefore we conclude that for any given input u and any two different $c_m, c_n \in [0, c^-_{s,\max}]$, the following expression holds:

$$\text{sgn}(h(c_m,u) - h(c_n,u)) = \text{sgn}(c_m - c_n), \quad (22)$$

where operator $\text{sgn}(\cdot)$ is the signum function.

Remark 2. Let $F(x) = \begin{bmatrix} f_1(x) & f_2(x) & ... & f_{N-1}(x) \end{bmatrix}^T$. It is evident that $F(x)$ is continuously differentiable with respect to the states, a sufficient condition for Lipschitz continuity [20]. For any two vectors $z_1, z_2 \in \mathbb{R}^{N-1}$, where each entry of z_1 and z_2 is in $[0, c^-_{s,\max}]$, a Lipschitz constant can be obtained by computing the infinity norm of $\partial F/\partial x$, i.e., $K = \|\partial F/\partial x\|_\infty$, so that

$$\|F(z_1) - F(z_2)\| \le K\|z_1 - z_2\|. \quad (23)$$

Remark 3. Note that $f_N(c_{N-1}, c_N, u)$ in (21) is bounded within the compact operating interval $c_{N-1}, c_N \in [0, c^-_{s,\max}]$ as long as the current density i_n is finite. Mathematically, for any two points (c_{N-1}, c_N), $(c^*_{N-1}, c^*_N) \in [0, c^-_{s,\max}] \times [0, c^-_{s,\max}]$,

$$|f_N(c_{N-1}, c_N, u) - f_N(c^*_{N-1}, c^*_N, u)| \le M, \quad (24)$$

where $0 < M < \infty$.

C. Nonlinear Observer Design

In this section, we detail the observer design for model (18) utilizing the equivalent control concept. As one may observe, mathematically, the input u only appears in the dynamics of c_N. We first seek to estimate the state of the forced c_N subsystem, and the estimation of rest of states c_1 to c_{N-1} is based on an autonomous subsystem with estimated c_N being the output signal for those subsystems.

We separate state x into two parts, $x = \begin{bmatrix} \xi^T & c_N \end{bmatrix}^T$, where $\xi = \begin{bmatrix} c_1 & c_2 & \cdots & c_{N-1} \end{bmatrix}^T$, and consider the following observer structure:

$$\dot{\hat{\xi}} = \overline{\mathcal{A}}\hat{\xi} + F(\hat{\xi}) + L^*(t)v, \quad (25)$$

$$\dot{\hat{c}}_N = \tau\frac{N-1}{N}\hat{c}_{N-1} - \tau\frac{N-1}{N}\hat{c}_N + \tau\theta\hat{f}_N + L\cdot\text{sgn}(y-\hat{y}) \quad (26)$$

$$\hat{y} = h(\hat{c}_N, u), \quad (27)$$

where scalar observer gain $L > 0$ and time-varying observer gain vector $L^*(t) \in \mathbb{R}^{N-1}$ are to be designed. The estimated states $\hat{\xi} = \begin{bmatrix} \hat{c}_1 & \hat{c}_2 & \cdots & \hat{c}_{N-1} \end{bmatrix}^T$, and $\overline{\mathcal{A}}$ is the matrix $\mathcal{A}$ excluding the last row and last column. v is the filtered version of $L\cdot\text{sgn}(y-\hat{y})$. Furthermore, $\hat{f}_N \triangleq f(\hat{c}_{N-1}, \hat{c}_N, u)$.

D. Observer Convergence Analysis

We first present the convergence analysis of the observer (26) in the following Lemma.

Lemma 1. *Consider the surface concentration dynamics (17) and estimated surface concentration from observer (26). If the scalar observer gain L verifies*

$$L > \tau\frac{N-1}{N}|\tilde{c}_{N-1}|_{max} + \tau\theta M, \quad (28)$$

where $|\tilde{c}_{N-1}|_{max}$ is the maximum absolute error of c_{N-1} estimation, then the estimation error $\tilde{c}_N = c_N - \hat{c}_N$ converges to zero in finite time.

Proof: Consider the estimation error $\tilde{c}_N = c_N - \hat{c}_N$. Subtracting (26) from (18), and the error dynamics can be written as:

$$\dot{\tilde{c}}_N = \tau\frac{N-1}{N}\tilde{c}_{N-1} - \tau\frac{N-1}{N}\tilde{c}_N + \tau\theta\tilde{f}_N - L\text{sgn}(\tilde{c}_N), \quad (29)$$

where $\tilde{f}_N = f_N(c_{N-1}, c_N, u) - f_N(\hat{c}_{N-1}, \hat{c}_N, u)$. Note that we utilize the monotonicity property of y (see Assumption 1) to substitute $\text{sgn}(\tilde{y})$ with $\text{sgn}(\tilde{c}_N)$. We analyze error dynamics (29) using the Lyapunov function $V_1 = \frac{1}{2}\tilde{c}_N^2$, and the derivative of V_1 along the trajectory of $\tilde{c}_N$ is

$$\begin{aligned}\dot{V}_1 &= \tilde{c}_N \dot{\tilde{c}}_N \\ &= \tilde{c}_N \left(\tau \frac{N-1}{N} \tilde{c}_{N-1} - \tau \frac{N-1}{N} \tilde{c}_N + \tau\theta \tilde{f}_N - L\text{sgn}(\tilde{c}_N) \right) \\ &\leq \tau |\tilde{c}_N| \left(\frac{N-1}{N} |\tilde{c}_{N-1}| + \theta |\tilde{f}_N| \right) - L|\tilde{c}_N| - \tau \frac{N-1}{N} \tilde{c}_N^2 \\ &\leq |\tilde{c}_N| \left(\tau \frac{N-1}{N} |\tilde{c}_{N-1}| + \tau\theta M - L \right). \end{aligned} \tag{30}$$

If the gain L is chosen high enough such that

$$L > \tau \frac{N-1}{N} |\tilde{c}_{N-1}|_{\max} + \tau\theta M, \tag{31}$$

then we have that $\dot{V}_1 \leq 0$. Therefore it can be concluded that $\tilde{c}_N \to 0$ in finte time [21], and the sliding mode is attained. At the sliding mode, we have $\tilde{c}_N = 0$ and $\dot{\tilde{c}}_N = 0$. Substituting these expressions in (29), we can write

$$v = \tau \frac{N-1}{N} \tilde{c}_{N-1} + \tau\theta \tilde{f}_N \triangleq \kappa(t) C \tilde{\xi}, \tag{32}$$

where

$$\begin{aligned}\kappa(t) =& \tau \frac{N-1}{N} + \tau\theta \frac{N-2}{2N} c_N + \frac{1}{2}\tau\theta \frac{i_n \cdot \Delta r}{D \cdot F \cdot (1 + \theta c_N)} \\ &+ \frac{1}{4}\tau\theta (c_{N-1} + \hat{c}_{N-1}), \end{aligned} \tag{33}$$

$$C = \begin{bmatrix} 0 & 0 & \cdots & 0 & 1 \end{bmatrix} \in \mathbb{R}^{1 \times (N-1)}. \tag{34}$$

Remark 4. Note that the coefficient $\kappa(t)$ is a time-varying function. We can re-write $L^*(t)$ as $L^*(t) = L^\dagger / \kappa(t)$, where $L^\dagger \in \mathbb{R}^{N-1}$ is a scalar vector, to cancel the time-varying term $\kappa(t)$ in v. In this way, the design parameter in observer (25) becomes time-invariant vector $L^\dagger$.

The following theorem provides the convergence condition of the observer (25) and (26).

Theorem 2. *Consider the plant model (18) with state observer (25) and (26), where function $F(X)$ is Lipschitz continuous with Lipschitz constant K. If there exists gain vector $L^\dagger$ and a positive definite matrix Q such that*

$$(\overline{\mathcal{A}} - L^\dagger C)^T + (\overline{\mathcal{A}} - L^\dagger C) = -Q, \tag{35}$$

$$\lambda_{\min}(Q) > 2K, \tag{36}$$

where $\lambda_{min}(Q)$ denotes the minimum eigenvalue of Q, along with the properly selected scalar gain L as stated in Lemma 1, then the state estimation error $\tilde{c}_N$ converges to zero in finite time and $\tilde{\xi} = \xi - \hat{\xi}$ converges to zero exponentially.

Proof: The convergence of observer (26) has been proved in Lemma 1. Subtracting (25) from (18), the estimation error dynamics of $\tilde{\xi} = \xi - \hat{\xi}$ can be written as

$$\dot{\tilde{\xi}} = (\overline{\mathcal{A}} - L^\dagger C)\tilde{\xi} + F(\xi) - F(\hat{\xi}). \tag{37}$$

Choose the Lyapunov function candidate $V_2 = \tilde{\xi}^T \tilde{\xi}$, and the derivative of V_2 is

$$\begin{aligned}\dot{V}_2 &= \dot{\tilde{\xi}}^T \tilde{\xi} + \tilde{\xi}^T \dot{\tilde{\xi}} \\ &= \tilde{\xi}^T [(\overline{\mathcal{A}} - L^\dagger C)^T + (\overline{\mathcal{A}} - L^\dagger C)] \tilde{\xi} + 2\tilde{\xi}^T [F(\xi) - F(\hat{\xi})] \\ &= -\tilde{\xi}^T Q \tilde{\xi} + 2\tilde{\xi}^T [F(\xi) - F(\hat{\xi})] \\ &\leq -\lambda_{\min}(Q) \|\tilde{\xi}\|^2 + 2\|\tilde{\xi}\| \cdot K \|\tilde{\xi}\| \\ &= -\tilde{\xi}^T (\lambda_{\min}(Q) - 2K) \tilde{\xi}. \end{aligned} \tag{38}$$

Define $R \triangleq \lambda_{\min}(Q) - 2K$, and rewrite Eq. (38) as

$$\dot{V}_2 \leq -R \cdot \tilde{\xi}^T \tilde{\xi} \leq -R V_2. \tag{39}$$

Integrating Eq. (39) over an closed interval $\left[t_0, t\right]$ shows that $\tilde{\xi}$ has exponential decay according to

$$\|\tilde{\xi}(t)\| \leq \|\tilde{\xi}(t_0)\| e^{-\frac{1}{2}R(t-t_0)}, \tag{40}$$

from which we conclude that the estimation error $\tilde{\xi}$ approaches zero exponentially as $t \to \infty$.

IV. Simulation Results and Discussion

We present numerical simulation results that demonstrate the observer performance. The parameters used in the simulation studies are adopted from the DUALFOIL simulation package that is publicly available [22]. The mechanical parameters for graphite anode are $E_n = 60$GPa, $\nu_n = 0.25$, and $\Omega_n = 4.926 \times 10^{-6}$m^3/mol [12]. We illustrate the observer performance by initializing the state estimates at incorrect values.

We apply an electric vehicle-like charge-discharge cycle to imitate real-world driving scenarios. This input current signal is generated by concatenating two Urban Dynamometer Driving Schedule (UDDS) drive cycles, which is a highly transient input with large C-rate magnitude. Figure 2 portrays the evolution of current, lithium ion surface concentration, voltage, and bulk SOC in the plant simulation generated by (6), as well as their estimated values from nonlinear observer (25)-(27). It also provides the plot of maximum radial and tangential stresses over time, which are located at the center and the surface of the particle, respectively [15], [17]. The lithium ion surface concentration is initialized with 15% error. The bulk SOC used in this work is defined as the normalized average over spherical coordinates:

$$SOC(t) = \frac{3}{(R_s^-)^3 c_{s,max}^-} \int_0^{R_s^-} r^2 c_s^-(r,t) dr. \tag{41}$$

With an appropriate choice of gain as presented in Section III-C, the estimates effectively converge to their true values. It is worth mentioning that the internal radial stress can be monitored in real time to prevent it from getting higher than the yielding stress of the electrode material.

V. Conclusion

This paper presents a nonlinear observer for mechanical stress estimation in lithium-ion batteries, along with solid phase lithium ion concentration - i.e. state-of-charge. A key feature is utilizing a single particle model coupled with

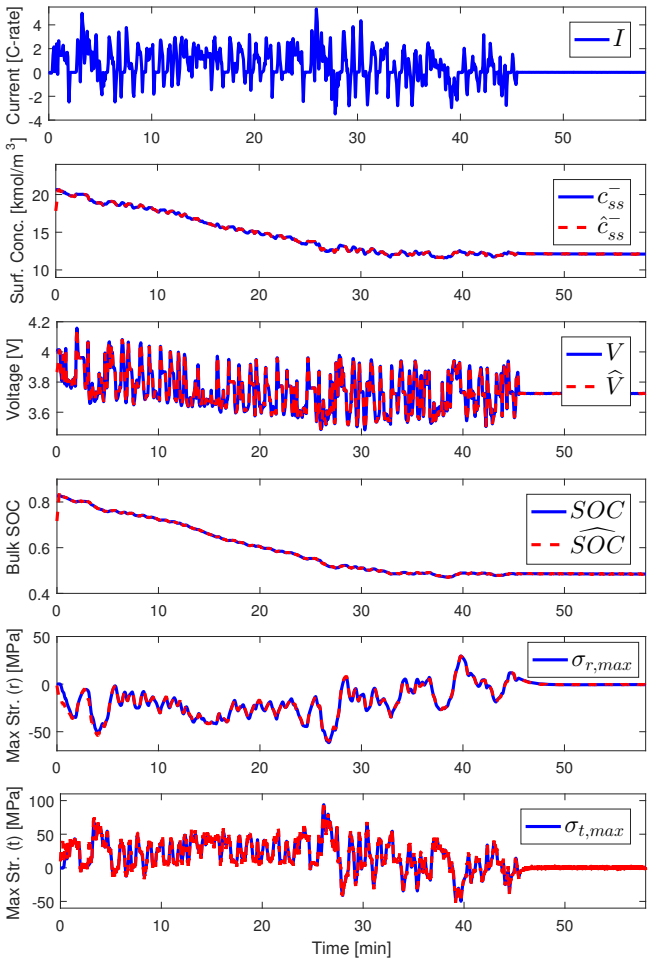

Fig. 2: Evolution of state estimation for UDDS$\times$2 charge-discharge cycle. The estimates of states are initialized with incorrect values.

an intercalation-induced stress model. A model reduction technique is applied to express the equilibrium of the cathode states in terms of anode states, to achieve observability. The reduced system is further approximated by nonlinear ODEs using the finite difference method. A nonlinear observer based on the equivalent control concept is proposed for estimating the states from current and voltage measurements. The observer's convergence is mathematically proven using Lyapunov stability theory. Real-time monitoring of internal mechanical stress enables a battery management system to apply optimal control methods that protect against particle fracture, and consequently extend battery life. Simulation study demonstrates observer performances.

References

[1] N. A. Chaturvedi, R. Klein, J. Christensen, J. Ahmed, and A. Kojic, "Algorithms for advanced battery-management systems," *IEEE Control Systems*, vol. 30, no. 3, pp. 49–68, 2010.

[3] S. Santhanagopalan, Q. Guo, P. Ramadass, and R. E. White, "Review of models for predicting the cycling performance of lithium ion batteries," *Journal of Power Sources*, vol. 156, no. 2, pp. 620–628, 2006.

[2] M. Doyle, T. F. Fuller, and J. Newman, "Modeling of galvanostatic charge and discharge of the lithium/polymer/insertion cell," *Journal of the Electrochemical Society*, vol. 140, no. 6, pp. 1526–1533, 1993.

[4] S. Santhanagopalan and R. E. White, "Online estimation of the state of charge of a lithium ion cell," *Journal of power sources*, vol. 161, no. 2, pp. 1346–1355, 2006.

[5] D. Di Domenico, A. Stefanopoulou, and G. Fiengo, "Lithium-ion battery state of charge and critical surface charge estimation using an electrochemical model-based extended kalman filter," *Journal of dynamic systems, measurement, and control*, vol. 132, no. 6, p. 061302, 2010.

[6] S. J. Moura, N. Chaturvedi, and M. Krstic, "Adaptive pde observer for battery soc/soh estimation," in *2012 ASME Dynamic Systems and Control Conference*, 2012.

[7] S. K. Rahimian, S. Rayman, and R. E. White, "Extension of physics-based single particle model for higher charge–discharge rates," *Journal of Power Sources*, vol. 224, pp. 180–194, 2013.

[8] W. Luo, C. Lyu, L. Wang, and L. Zhang, "An approximate solution for electrolyte concentration distribution in physics-based lithium-ion cell models," *Microelectronics Reliability*, vol. 53, no. 6, pp. 797–804, 2013.

[9] S. J. Moura, F. B. Argomedo, R. Klein, A. Mirtabatabaei, and M. Krstic, "Battery state estimation for a single particle model with electrolyte dynamics," *IEEE Transactions on Control Systems Technology*, vol. 25, no. 2, pp. 453–468, 2017.

[10] A. Barré, B. Deguilhem, S. Grolleau, M. Gérard, F. Suard, and D. Riu, "A review on lithium-ion battery ageing mechanisms and estimations for automotive applications," *Journal of Power Sources*, vol. 241, pp. 680–689, 2013.

[11] S. Kalnaus, K. Rhodes, and C. Daniel, "A study of lithium ion intercalation induced fracture of silicon particles used as anode material in li-ion battery," *Journal of Power Sources*, vol. 196, no. 19, pp. 8116–8124, 2011.

[12] J. Li, N. Lotfi, R. Landers, and J. Park, "A single particle model for lithium-ion batteries with electrolyte and stress-enhanced diffusion physics," *Journal of The Electrochemical Society*, vol. 164, no. 4, pp. A874–A883, 2017.

[13] B. Suthar, V. Ramadesigan, S. De, R. D. Braatz, and V. R. Subramanian, "Optimal charging profiles for mechanically constrained lithium-ion batteries," *Physical Chemistry Chemical Physics*, vol. 16, no. 1, pp. 277–287, 2014.

[14] K. Aifantis and J. Dempsey, "Stable crack growth in nanostructured li-batteries," *Journal of power sources*, vol. 143, no. 1, pp. 203–211, 2005.

[15] R. Deshpande, Y. Qi, and Y.-T. Cheng, "Effects of concentration-dependent elastic modulus on diffusion-induced stresses for battery applications," *Journal of the Electrochemical Society*, vol. 157, no. 8, pp. A967–A971, 2010.

[16] J. Christensen and J. Newman, "Stress generation and fracture in lithium insertion materials," *Journal of Solid State Electrochemistry*, vol. 10, no. 5, pp. 293–319, 2006.

[17] X. Zhang, W. Shyy, and A. M. Sastry, "Numerical simulation of intercalation-induced stress in li-ion battery electrode particles," *Journal of the Electrochemical Society*, vol. 154, no. 10, pp. A910–A916, 2007.

[18] K. E. Thomas, J. Newman, and R. M. Darling, "Mathematical modeling of lithium batteries," in *Advances in lithium-ion batteries*, pp. 345–392, Springer, 2002.

[19] C.-T. Chen, *Linear system theory and design*. Oxford University Press, Inc., 1995.

[20] S. Dey, B. Ayalew, and P. Pisu, "Nonlinear robust observers for state-of-charge estimation of lithium-ion cells based on a reduced electrochemical model," *IEEE Transactions on Control Systems Technology*, vol. 23, no. 5, pp. 1935–1942, 2015.

[21] D. Zhang, S. Dey, H. E. Perez, and S. J. Moura, "Remaining useful life estimation of lithium-ion batteries based on thermal dynamics," in *American Control Conference (ACC), 2017*, pp. 4042–4047, IEEE, 2017.

[22] J. Newman, "Fortran programs for simulation of electrochemical systems," 2008.